*Journal of Power Sources, 43–44* (1993) 169–180 

# Metal deposition and dissolution monitored by *in situ* scanning tunneling microscopy

U. Stimming and R. Vogel
*Institute of Energy Process Engineering, Research Center Jülich, D-5170 Jülich (Germany)*
D. M. Kolb and T. Will
*Department of Electrochemistry, University of Ulm, Albert-Einstein-Allee 11, D-7900 Ulm (Germany)*

**Abstract**

The possibilities of scanning tunneling microscopy (STM) for the study of metal deposition and dissolution reactions under *in situ* electrochemical conditions will be described and illustrated by examples. The metal reaction being studied is copper deposition and dissolution on foreign substrates such as Au(111), or polycrystalline copper. Data on atomically-resolved copper adlayers and on bulk copper deposition on gold will be presented. In addition, time resolved *in situ* STM for the study of copper deposition and dissolution on polycrystalline copper will be shown as well. From the latter local reaction rates can be estimated. The necessity to consider a possible influence of the tip on the results will be emphasized and the reasons for such an interference of the tip will be briefly discussed.

## Introduction

Metal deposition and dissolution processes in electrochemical systems are usually studied by techniques involving measurements of potential, current and charge. From such information deposition rates can be derived. Although much effort has been put into the elucidation of the mechanisms of metal deposition and dissolution, the conclusions derived from experiments have always been indirect since they either refer to averaged quantities such as current, or to *ex situ* techniques such as electron microscopies or surface science techniques. The advent of scanning tunneling microscopy [1] allows one to study surfaces in real space and under *in situ* electrochemical conditions [2–4].

In the following, the application of scanning tunneling microscopy (STM) for the study of copper deposition and dissolution on foreign substrates, such as single crystalline gold electrodes and on polycrystalline copper, will be illustrated. The results demonstrate that *in situ* STM is a valuable technique for the study of such electrochemical processes.

One has to consider, however, that the presence of the probing tip in the electrochemical cell represents a modification of the electrochemical environment. This modification has to be fully understood in order to derive kinetic information from STM results in electrochemical cells.

0378-7753/93/$6.00 

**Copper deposition on Au(111)**

The electrochemical behaviour of a gold electrode in a $Cu^{2+}$-containing electrolyte can be divided into four regimes, as shown by a cyclic voltammogram of Au(111) in 0.1 M $H_2SO_4 + 1 \times 10^{-3}$ M $CuSO_4$, taken in an STM cell (Fig. 1):

(i) the double-layer region (I), where no faradaic processes occur;

(ii) the range of surface oxide formation (II) and reduction of the surface oxide (II');

(iii) the range of underpotential deposition (UPD) [5], where a monolayer of copper adsorbs (III) and desorbs (III') from the surface, and,

(iv) the range of bulk copper deposition (IV) and dissolution (IV').

The exact shape of the voltammetric curve can vary with the electrolyte composition and also with surface orientation; the main features remain, however, essentially unaltered. Hence, the changes of the electrode surface associated with these features may readily be exemplified by studying a Au(111) surface in $Cu^{2+}$-containing electrolyte at different potentials.

When, after surface preparation [6], the Au(111) electrode is immersed at a potential within the double-layer region and held there, the typical morphology of the Au(111) surface is observed (Fig. 2(a)). Its characteristic features are large, atomically-flat terraces, separated by monoatomic steps, and some small gold islands of monoatomic height. The step in the front part of Fig. 2(a) starts at a screw dislocation and meanders over the surface, whereas the step lines in the back of the image run straight along the main crystallographic directions of the (111) surface and enclose angles of 60°. Though individual kinks are below the lateral resolution of the rather large area image of Fig. 2(a), it is plausible to expect a much higher density of kink sites at the meandering step as compared with the straight ones. We will come back to this point later.

Comparable images were obtained in electrolytes without copper ions [6]. This similarity indicates that, within the double-layer range, there is no close interaction between the electrode and the copper ions in solution.

A direct proof for the absence of any copper deposit on the surface is derived from imaging the flat terraces with atomic resolution (Fig. 2(b)), which yields the

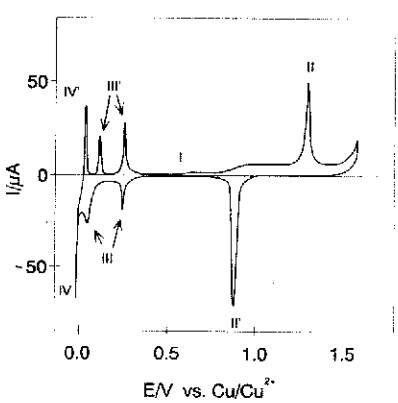


Fig. 1. Cyclic voltammetry of Au(111) in 0.1 M $H_2SO_4 + 1 \times 10^{-3}$ M $CuSO_4$, recorded in an STM cell.

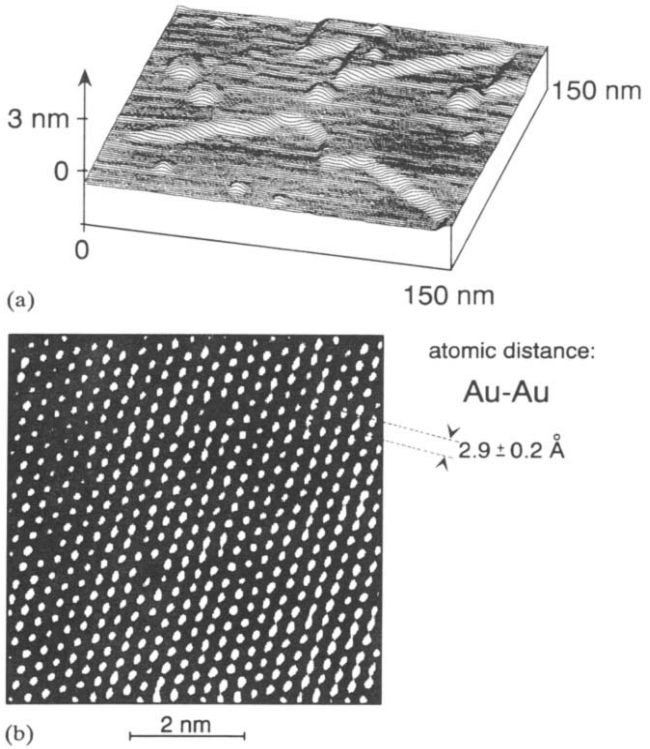


Fig. 2. STM images of Au(111): (a) typical surface morphology, recorded in $5\times10^{-3}$ M $H_2SO_4+5\times10^{-5}$ M $CuSO_4$ at +300 mV vs. $Cu/Cu^{2+}$, and (b) atomic resolution image of the bare surface, recorded 0.5 M $H_2SO_4+5\times10^{-3}$ M $CuSO_4$ at +600 mV vs. $Cu/Cu^{2+}$. (Reproduced from ref. 8 with permission from the Royal Society of Chemistry.)

hexagonal arrangement of individual gold atoms which is characteristic of the Au(111) surface [7, 8].

At potentials positive from the double layer region, surface oxide formation is known to occur. Oxidation of the electrode forces surface oxygen atoms to exchange places with gold atoms, resulting in the formation of gold oxide. Subsequent reduction can lead to a substantial roughening of the surface. When the potential is subsequently held in the double-layer region, surface diffusion causes a slow reordering of this roughened surface. Such roughening and annealing processes have been studied by several authors on various metals [9–14], and thus details will not be discussed here. We would rather focus on the point, that for the case discussed, structural changes are involved, which are not accompanied by any charge flow. Hence, real space imaging is mandatory if one wants to gain information about such processes. To illustrate this, Fig. 3(a) shows an image of a severely roughened Au(111) surface immediately after the potential was returned to the double-layer region. After one hour at the same potential (Fig. 3(b)), the roughness has already significantly decreased, and an additional hour later (Fig. 3(c)) the surface is almost as smooth as it was in the beginning.

At potentials negative from the double-layer region, within the UPD range, no apparent changes of surface morphology were observed, as far as the shape of terraces and steps is concerned. This is in agreement with the expectation of adsorption and

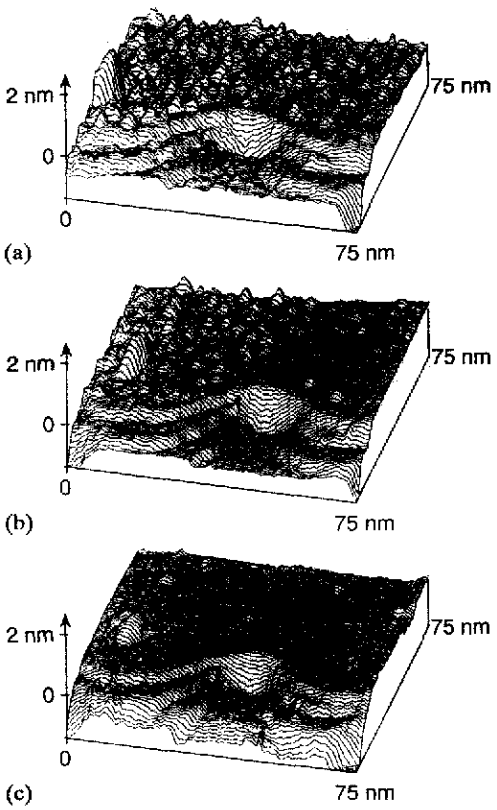


Fig. 3. STM images of roughened Au(111) after oxidation/reduction cycles in $5\times10^{-3}$ M $H_2SO_4+5\times10^{-5}$ M $CuSO_4$, recorded at 750 mV vs. $Cu/Cu^{2+}$: (a) immediately after roughening, (b) 1 h later, and (c) 2 h later.

desorption of a copper monolayer, which homogeneously covers the electrode and reproduces the morphology of the underlying substrate. Only when atomic resolution is obtained, changes of surface condition within the UPD range [15, 16] become visible. Copper adsorbs on Au(111) in the form of a well-ordered overlayer. The structure of the overlayer depends on coverage and is strongly affected by the nature of coadsorbed anions. In sulfuric acid, where the anions are intermediately strongly adsorbing sulfate or bisulfate ions, the formation of a full $(1\times1)$-overlayer is preceded by a $(\sqrt{3}\times\sqrt{3})R30°$ adlayer with a saturation coverage of 1/3 [17]. This adlayer is stable in the potential range between 205 and 50 mV, and, due to its large lattice constants, can readily be resolved with the STM. An image of copper atoms arranged in such a $(\sqrt{3}\times\sqrt{3})R30°$ adlattice is shown in Fig. 4.

Negative from the Nernst potential of $Cu/Cu^{2+}$, bulk deposition of copper occurs. Bulk deposition is an activated process of nucleation and growth, with a noticeable overvoltage required for nucleation. Once nuclei are formed, the crystallites grow very fast, which makes it difficult to follow the early stages of deposition with the STM quantitatively [18].

An image recorded in the course of copper deposition is presented in Fig. 5, which shows the same surface area as in Fig. 2(a). A comparison of both images

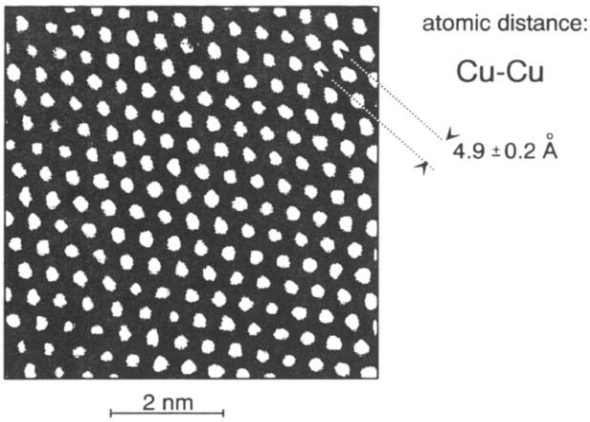


Fig. 4. STM image of Au(111), covered with 1/3 monolayer of copper atoms arranged in a $(\sqrt{3}\times\sqrt{3})R30°$ adlattice, recorded in 0.5 M $H_2SO_4 + 5\times10^{-3}$ M $CuSO_4$ at +150 mV vs. $Cu/Cu^{2+}$. (Reproduced from ref. 8 with permission from the Royal Society of Chemistry.)

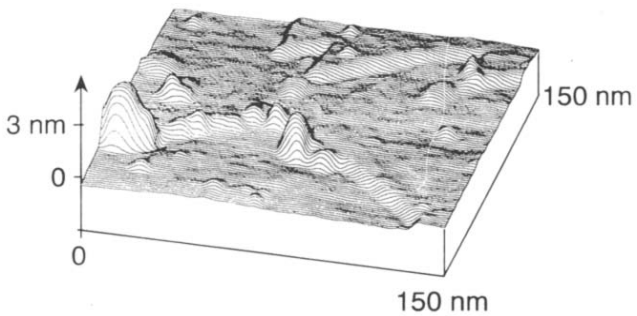


Fig. 5. STM image of Au(111) in $5\times10^{-3}$ M $H_2SO_4 + 5\times10^{-5}$ M $CuSO_4$ during bulk deposition of copper at −300 mV vs. $Cu/Cu^{2+}$; same surface area as in Fig. 2(a) is shown. (Reproduced from ref. 8 with permission from the Royal Society of Chemistry.)

allows one to distinguish the copper deposit from the substrate structure. In the back part of the image, where the step lines run straight, hardly any change is visible, though Fig. 2(a) shows the bare gold surface and in Fig. 5 at least a monolayer of copper must be present. This confirms the finding, that the underpotentially-deposited monolayer exactly reproduces the substrate structure as pointed out above.

Along the curved step in the front part, several mound-shaped structures have appeared, which represent the copper deposit. The location of those mounds correlates with the regions, where the step line changes its direction, and hence must exhibit a high density of kink sites. An especially prominent mound is formed at the screw dislocation in the left of Fig. 5. The important role of surface defects for nuclei formation is hence directly visualized in real space with the STM.

As far as the coating properties of the deposit are concerned, these are not only determined by the nucleation, but also by the growth mechanism of the crystallites. From comparing area and height of the mounds in Fig. 5 it can be derived, that growth lateral to the surface is larger than that in the direction of the surface normal (though this finding is obscured in the Figs. by the enhancement of the vertical scale).

The ratio, however, is less than a factor of ten, and hence an inhomogeneous coating of the surface with large variations in film thickness can be expected, when the deposition proceeds.

Fluctuations of the film thickness are a common problem in metal plating. Plating solutions therefore often contain small amounts of organic additives, so-called brighteners and levellers, which are known to improve the coating properties of the deposit. The effect of such an additive, e.g. crystal violet, on the early stage of metal plating is derived from comparing Fig. 6(a) with Fig. 6(b).

Figure 6(a) again shows the 'bumpy' structure of copper nuclei in the absence of organic additives (note, however, the different axis scales for lateral and vertical displacement). Figure 6(b), recorded in the presence of crystal violet, shows crystallites of much larger area and less height. Although the interaction of the additive with substrate and deposit could not be resolved with atomic resolution as yet it becomes

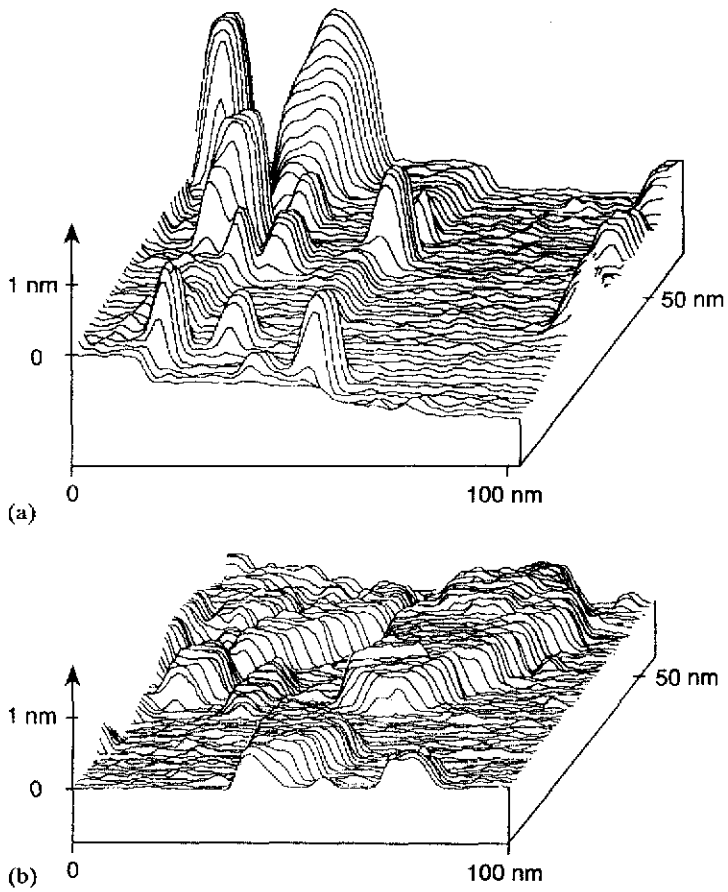


Fig. 6. STM images of Au(111) taken during the initial stages of copper bulk deposition: (a) in $1\times10^{-1}$ M $H_2SO_4+5\times10^{-5}$ M $CuSO_4$ at $-190$ mV vs. $Cu/Cu^{2+}$, and (b) in the same solution after adding $2.5\times10^{-5}$ M crystal violet at $-262$ mV vs. $Cu/Cu^{2+}$. (Reproduced from ref. 8 with permission from the Royal Society of Chemistry.)

clear, that the coadsorption of crystal violet increases the ratio between lateral spreading and vertical growth of the deposit by at least one order of magnitude. This results in a much more uniform coating of the surface.

**Copper deposition on and dissolution of polycrystalline copper**

STM operation requires the motion of an macroscopic piece of metal (the tip) with atomic precision, and, hence, is a rather slow method. The time required to record an image typically ranges from seconds to minutes. Thus, STM is usually used to image stable surface structures. However, dynamic processes occurring on the same time scale can readily be resolved in space and time, allowing the determination of local reaction rates and a comparison with the integral values derived from current/potential measurements.

To illustrate this possibility, a polycrystalline copper surface was imaged in dilute perchloric acid (pH=3) at different potentials relative to a copper wire in the same solution [19]. At open-circuit conditions, the potential is defined by the small amount of $Cu^{2+}$ ions induced to the solution by open-circuit corrosion (which, at pH=3, was found to induce no changes in surface morphology on the time scale of minutes [20]). At negative polarization down to −0.6 V, only a small cathodic current was observed due to reduction of minor amounts of residual oxygen and diffusion-limited copper deposition. At positive polarization, copper dissolves.

STM images were recorded under steady-state positive and negative polarization of the copper electrode in the potential range +50 mV to −0.6 V relative to the copper reference electrode. At each potential, an area of 16 nm×16 nm was imaged continuously. The time required to record an image was 7 s.

A sequence of images taken at −0.6 V is shown in Fig. 7. Here, nucleation and growth of a copper crystallite are visible in the lower part of the images. Because the images were recorded at equidistant time intervals of 7 s, the difference between subsequent frames directly reflects the rate of copper deposition or dissolution at the interface. As can easily be seen, this rate is fluctuating with time, and, from (B) through (F), even changes sign. This means, that copper seems to dissolve in spite of the strong negative polarization. Towards the end of the sequence, a second nucleus appears at the left of the first one.

At a small positive overpotential of 50 mV, as expected, copper dissolves, as shown by the recessing slope in the right part of the images of Fig. 8. In the upper left, however, after some time nucleation and growth of a copper crystallite occurs though the potential is positive, and though dissolution proceeds on the right side. Such a simultaneous occurrence of anodic and cathodic reactions can be understood from a kinetic derivation of the equilibrium potential which implies, that close to, but not at the equilibrium, the respective opposite reaction takes place with a small, but not negligible reaction rate. This situation is obviously observed in Fig. 8, where in spite of the overwhelming local anodic dissolution rate of ~100 mA/cm$^2$ the cathodic deposition reaction with a local deposition rate of −0.3 mA/cm$^2$ can be observed as well. These local current densities are estimated, according to Faraday's law, from the changes in surface morphology. For both Figs. 7 and 8 the local current densities are about two decades larger than the macroscopic current, which flows through the cell.

Comparing Figs. 7 and 8, a potential dependence of crystal growth behaviour can be derived: far from equilibrium (Fig. 7), the crystallite grows strictly three dimensional,

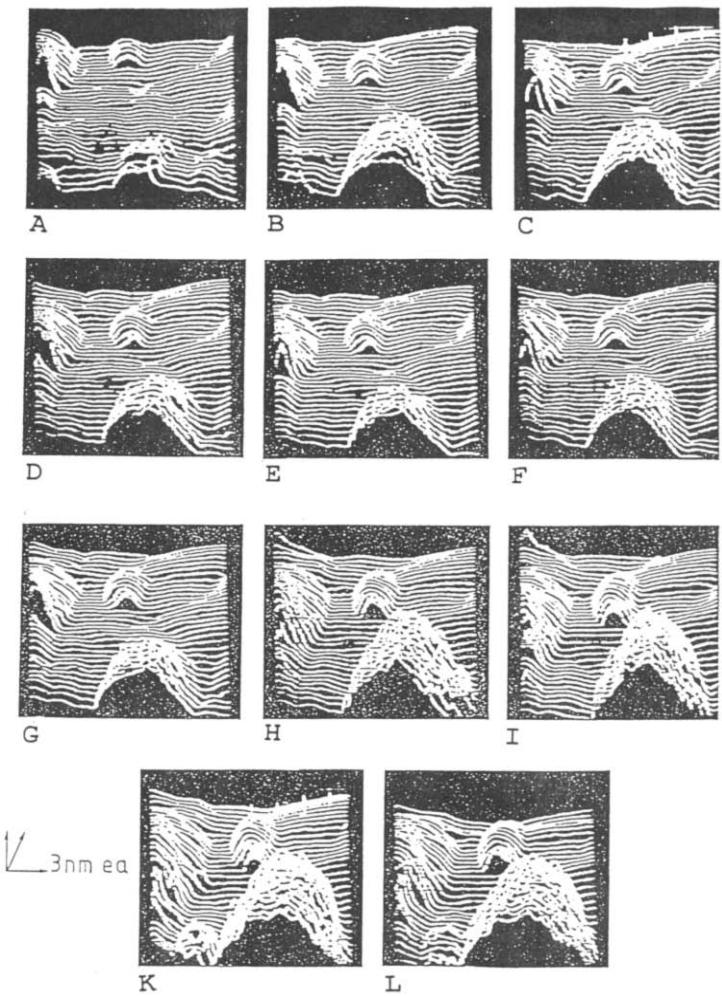


Fig. 7. Sequence of images of polycrystalline copper in $1\times10^{-3}$ M $HClO_4$ at $-0.6$ V vs. a copper wire in the same solution: (A) $t=0$ s (arbitrarily chosen); (B) $t=7$ s; (C) $t=14$ s; (D) $t=21$ s; (E) $t=28$ s; (F) $t=35$ s; (G) $t=42$ s; (H) $t=49$ s; (I) $t=56$ s; (K) $t=63$ s, and (L) $t=70$ s. (Reproduced from ref. 19.)

while close to the Nernst potential (Fig. 8) lateral spreading of the deposit dominates and results in a plateau shape.

## The influence of the tip

With electrochemical applications of STM, one always has to bear in mind that the surface region under investigation is distinguished from the rest of the electrode surface by the close proximity of the tip, which is introduced as a fourth electrode into the usual cell design.

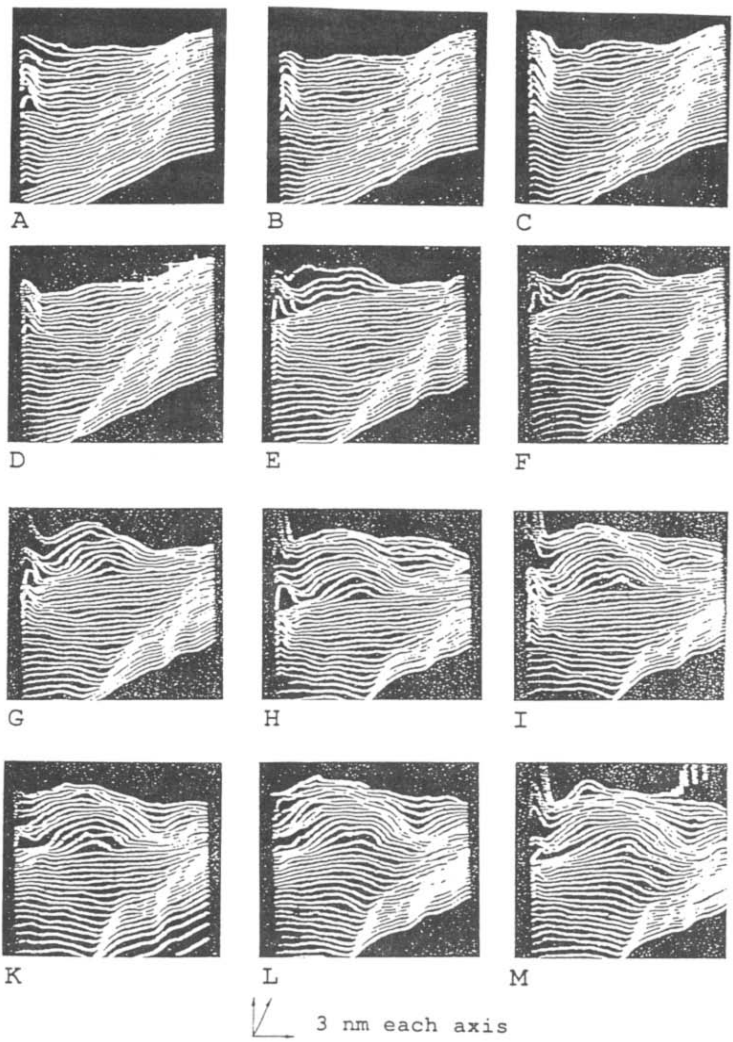


Fig. 8. Sequence of images of polycrystalline copper in $1\times10^{-3}$ M $HClO_4$ at +50 mV vs. a copper wire in the same solution: (A) $t=0$ (arbitrarily chosen); (B) $t=14$ s; (C) $t=28$ s; (D) $t=42$ s; (E) $t=140$ s; (F) $t=154$ s; (G) $t=168$ s; (H) $t=182$ s; (I) $t=196$ s; (K) $t=210$ s; (L) $t=224$ s, and (M) $t=238$ s. (Reproduced from ref. 19.)

So, several findings were noticed during the study of copper deposition on gold, which indicate a marked influence of the tip on the deposition process. Unusually high overpotentials of several hundred mV were required to induce nuclei formation under the tip, and the growth of these nuclei ceased after a few minutes. These are indications of a severe shielding effect of the tip. An example is shown in Fig. 9. At a potential where bulk deposition of copper on Au(111) should occur, a surface area of 100 nm$\times$100 nm (centre of Fig. 9) was scanned continuously the tip being held at a high positive potential. No major changes in surface morphology were observed although bulk deposition was expected. Subsequent doubling of the scan size revealed,

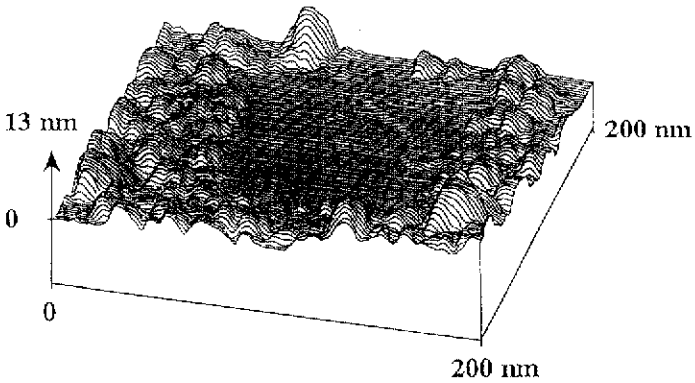


Fig. 9. STM image of Au(111) demonstrating the shielding effect of a positive tip potential on the bulk copper deposition in $5\times10^{-3}$ M $H_2SO_4+5\times10^{-5}$ M $CuSO_4$ at $-375$ mV vs. $Cu/Cu^{2+}$.

that the suppression of the copper deposition was restricted to the formerly-scanned area.

This suppression seems to depend on the tip potential, becoming more pronounced with increasingly positive potential of the tip. However, the effect shows a variation for different tips, indicating that the tip condition (e.g., shape) plays an important role. The elucidation of this effect deserves further clarification.

A possible explanation is, that the tip and the substrate form a local thin-layer cell in the region, which is scanned, and hence depletion of $Cu^{2+}$ ions within this layer and a nonuniform current distribution may have to be considered.

In order to investigate this problem, simulations of the distribution of the faradaic current (tunnel currents have been excluded) in the vicinity of the tunneling tip have been performed. The tip was modelled as a cone with an opening angle of 30° which ends in a hemisphere of 1 $\mu$m radius, 2 nm above the electrode (Fig. 10(a)). The tip, e.g., platinum, was assumed to be at a positive potential, where copper deposition on the tip can be excluded. The counter electrode was assumed parallel to the sample at 250 $\mu$m distance. Assuming an exchange current density of 1 mA/cm$^2$ and an ohmic resistivity of 2000 $\Omega$ cm for the electrolyte, local values for current density and potential were calculated numerically from the linearized Butler–Volmer equation according to the multigrid techniques [21]. It was found that the local density of the faradaic current under the tip can become an order of magnitude lower than the macroscopic current density. The calculations are so far restricted to an area with a radius larger than one $\mu$m with respect to the centre of the tip. The deviations of the current closer to the centre and thus more relevant for the situation in Fig. 9 may be far more dramatic.

Such a shielding effect depends on the overall current which flows through the electrode. The calculations were thus carried out for different macroscopic current densities ranging from 10 to 200 mA/cm$^2$ (Fig. 10(b)). These preliminary results already indicate the special situation in an electrochemical STM cell, but other effects may also contribute to the shielding effects of the tip observed in Fig. 9.

## Conclusions

It has been shown that the employment of *in situ* scanning tunneling microscopy can be a very valuable approach for the study of metal deposition and dissolution

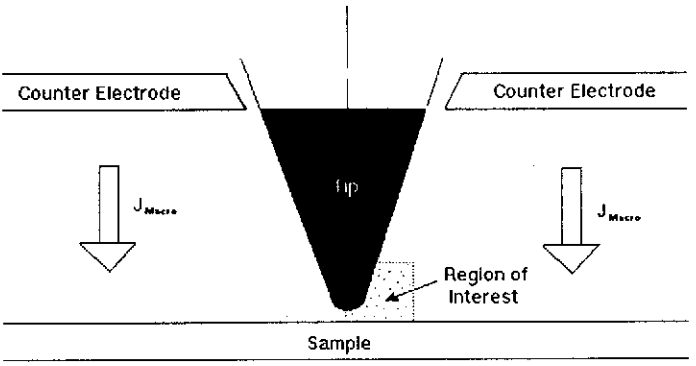


(a)

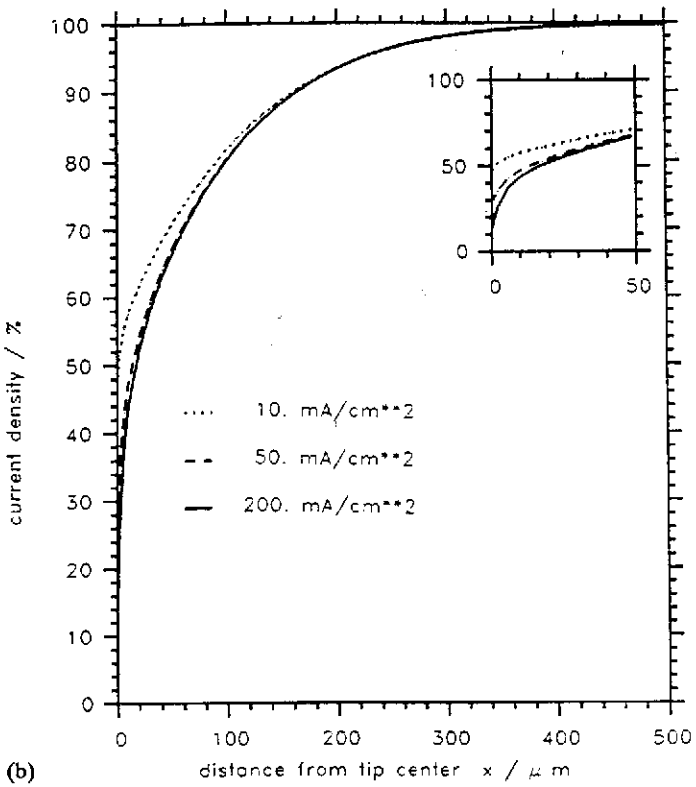


(b)

Fig. 10. (a) Schematic diagram of the model for calculation of the geometric shielding effect of the tip (not to scale; for parameters see text) and (b) distance dependence of the current for different current densities in the range 10 to 200 mA/cm$^2$.

reactions. STM offers the possibility to study the modifications of the surface induced by the deposition or dissolution reactions in real space. In addition, processes at electrode surfaces, which can be highly heterogeneous, are revealed by *in situ* imaging.

One has to consider, however, that the probing tip of the STM can interfere with the electrochemical process. In the future, such influences have to be considered more thoroughly in order to come to a precise assessment of the use of STM for the study of such processes.

## References


1 G. Binnig and H. Rohrer, *Helv. Phys. Acta, 55* (1982) 726.
2 P. K. Hansma and J. Tersoff, *J. Appl. Phys., 61* (1987) 1.
3 H. Siegenthaler and R. Christoph, in R. J. Behm, N. Garcia and H. Rohrer (eds.), *Scanning Tunneling Microscopy and Related Methods, NATO ASI Ser. E,* Vol. 184, Kluwer, Dordrecht, 1990, pp. 315–333.
4 T. R. I. Cataldi, I. G. Blackham, G. A. D. Briggs, J. B. Pethica and H. A. O. Hill, *J. Electroanal. Chem., 290* (1990) 1.
5 D. M. Kolb, in H. Gerischer, C. W. Tobias (eds.), *Advances in Electrochemistry and Electrochemical Engineering,* Vol. 11, Wiley–Interscience, New York, 1978, p. 125.
6 J. Wiechers, T. Twomey, D. M. Kolb and R. J. Behm, *J. Electroanal. Chem., 248* (1988) 451.
7 X. Gao, A. Hamelin and M. J. Weaver, *J. Chem. Phys., 95* (1991) 6993.
8 N. Batina, T. Will and D. M. Kolb, *Faraday Discuss. Chem. Soc., 94* (1993), in press.
9 D. J. Trevor, C. E. D. Chidsey and D. N. Loiacono, *Phys. Rev. Lett., 62* (1989) 451.
10 R. J. Nichols, O. M. Magnussen, J. Hotlos, T. Twomey, R. J. Behm and D. M. Kolb, *J. Electroanal. Chem., 290* (1990) 21.
11 K. Itaya, S. Sugawara, K. Sashikata and N. Furuya, *J. Vac. Sci. Technol. A, 8* (1990) 515.
12 H. Honbo, S. Sugawara and K. Itaya, *Anal. Chem., 62* (1990) 2424.
13 K. Sashikata, N. Furuya and K. Itaya, *J. Vac. Sci. Technol. B, 9* (1991) 457.
14 J.-S. Chen, T. M. Devine, D. F. Ogletree and M. Salmeron, *Surf. Sci., 258* (1991) 346.
15 O. M. Magnussen, J. Hotlos, R. J. Nichols, D. M. Kolb and R. J. Behm, *Phys. Rev. Lett., 64* (1990) 2929.
16 O. M. Magnussen, J. Hotlos, G. Beitel, D. M. Kolb and R. J. Behm, *J. Vac. Sci. Technol. B, 9* (1991) 969.
17 Y. Nakai, M. S. Zei, D. M. Kolb and G. Lehmpfuhl, *Ber. Bunsenges. Phys. Chem., 88* (1984) 340.
18 R. J. Nichols, W. Beckmann, H. Meyer, N. Batina and D. M. Kolb, *J. Electroanal. Chem.*, in press.
19 X. G. Zhang and U. Stimming, *J. Electroanal. Chem., 291* (1990) 273.
20 X. G. Zhang and U. Stimming, *Corros. Sci., 30* (1990) 951.
21 J. Divisek, R. Jung, B. Steffen and U. Stimming, personal communication.